

Numerical study of the needle inclination angle effect on the ionic wind direction

Ilya Elagin, Andrey Samusenko*, Vladimir A. Chirkov

St. Petersburg State University, 7/9 Universitetskaya nab., St. Petersburg, 199034, Russia

* Corresponding author: a.samusenko@spbu.ru (Andrey Samusenko)

Received: 20 December 2019

Revised: 12 March 2020

Accepted: 20 March 2020

Published online: 25 March 2020

Abstract

The effect of the inclination angle between the high voltage electrode (needle) and the grounded one (plane) on the ionic wind jet direction is considered. Ionic wind is induced by positive corona discharge. Experimental data (instantaneous velocity field observed using PIV-method) show that jet direction is defined primarily by the needle inclination. The computer simulation based on the finite element method allows one to reproduce both the current-voltage characteristics and the flow pattern with a good agreement and also facilitates a physical explanation of the strong influence of the needle inclination on the ionic wind direction.

Keywords: Computer simulation, corona discharge, Coulomb force, drift-diffusion approximation, electrohydrodynamic flow.

1. Introduction

Ionic wind is a gas flow caused by a corona discharge [1, 2]. The phenomenon is also referred to as electric or corona wind or electrohydrodynamic airflow and has wide application range for: the decontamination of liquids and gases [3, 4], intensive cooling of locally heated surface [5–8], airflow control [9–11], electrohydrodynamic pumping [12], and propulsion [13, 14], etc. The following expression is generally used for estimating the total force moving air in the ionic wind jet [15, 16]:

$$F_{iw} = \frac{Id}{\mu} - F_d \quad (1)$$

Here I is the total electric current of the corona discharge, d is the interelectrode distance, μ is the mobility of charge carriers (ions or electrons) in the air gap, F_d is the hydrodynamic drag force (it is frequently considered to be small in comparison with F_{iw} [16]). Equation (1) does not provide information about the jet direction; however, generally, the latter issue is quite a trivial one: the ionic wind jet is directed perpendicular to the plane in many simple electrode configurations, e.g., in wire- or needle-plane systems (see, e.g., [17, 18]). However, the situation changes when considering systems that do not have a plane or an axis of symmetry. Since the force acting on air is formed by momentum transfer from drifting charged particles to molecules, the direction of the ionic wind jet should be affected by the direction of the charged particles motion. Therefore, it can be assumed that the direction of the ionic wind jet can be varied. To achieve this, it is necessary to "force" the ion flow to move to the plane electrode not along the shortest path. In the case of the needle-plane system, the high-voltage electrode can be inclined concerning the plane. The needle inclination can be expected to yield the change in the direction of the electric wind jet since the maximum value of electric field strength and the maximum of the Coulomb volume force are observed near the tip of the pointed electrode. However, it is not obvious how the tilt of the needle affects the jet and whether the latter will be straightforward in such an electrode configuration.

The above issue is of special interest, in particular, when designing the devices for heat transfer enhancement since the phenomenon can let one improve thermal management and control heat fluxes to avoid their

overlapping, especially when cooling extended heat sources. Some original experimental data confirming the feasibility of the jet direction control can be found in [19].

2. Model description

A numerical simulation is an effective way to estimate the characteristics of a corona discharge and ionic wind. Usually, the corresponding computer models base on the finite element method implemented in specialized software packages. The unipolar approximation is often used [20–23], which quickens the solution process and claims for fewer resources in comparison with more complex treatments. However, the drift-diffusion approximation taking into account electrons, ions and ionization processes in corona sheath may also be used. The latter is more accurate in the description of base physical processes than the former though it is more resource intensive. Nevertheless, it was possible to implement the drift-diffusion model without reducing it to unipolar approximation in the considered system.

The corona discharge of positive polarity is chosen to investigate the effect of needle inclination angle on the ionic wind direction. The corresponding set of equations (2)–(6) is equivalent to the one considered in [24] and involves the Poisson's equation (2), the definition of the electric field (3), the Nernst-Planck (transport) equations for electrons (4) and positive ions (5), and the approximate equation (6) for photoionization rate S_{ph} (further details can be found in [25]). The latter equation was used in computer models of positive streamers [24] where spatial scales and the electric field strength are of the same orders of magnitude as those in a corona discharge.

$$\varepsilon_0 \nabla^2 \varphi = -e(n_i - n_e) \quad (2)$$

$$\mathbf{E} = -\nabla \varphi \quad (3)$$

$$\partial n_e / \partial t + \operatorname{div}(-D_e \nabla n_e - n_e \mu_e \mathbf{E}) = \alpha(E) \mu_e E n_e + S_{ph} \quad (4)$$

$$\partial n_i / \partial t + \operatorname{div}(-D_i \nabla n_i + n_i \mu_i \mathbf{E}) = \alpha(E) \mu_e E n_e + S_{ph} \quad (5)$$

$$-\nabla^2 S_{ph} = -k^2 S_{ph} + g k^2 \alpha(E) \mu_e E n_e \quad (6)$$

The unknown functions in the equation set (2)–(6) are the following: electric potential φ , concentrations of positive ions n_i and electrons n_e , and photoionization rate S_{ph} . $D_{i,e}$ are the ion and electron diffusion coefficients, $\mu_{i,e}$ are the ion and electron mobility values, e is the elementary charge, and ε_0 is the vacuum permittivity.

The dependences of electron mobility and diffusion coefficient on electric field strength are set in accordance with [26–28]. The dependence of the ionization coefficient α on the electric field strength E is given in accordance with the interpolating function $\alpha(E) = A \cdot \exp(-B/E)$ [26]. The ion mobility μ_i was set equal to $1.8 \times 10^{-4} \text{ m}^2 \cdot \text{V}^{-1} \cdot \text{s}^{-1}$; the value is used in [29] although some authors consider larger values (up to $3 \times 10^{-4} \text{ m}^2 \cdot \text{V}^{-1} \cdot \text{s}^{-1}$ [15]). Ion diffusion coefficient is set equal to $D_i = \mu_i k_B T / e = 8 \times 10^{-6} \text{ m}^2 \cdot \text{s}^{-1}$ where k_B is the Boltzmann constant, $T = 293 \text{ K}$. The dimensionless coefficient g characterizing the relationship between impact ionization and ionizing photons emission is equal to $p_q / (p + p_q) \cdot A_1 / \lambda_1$ according to [25] (here p is the air pressure, p_q is the so-called “quenching pressure”, λ_1 and A_1 are coefficients in interpolation of experimental data). The coefficient g is set equal to 5×10^{-5} whereas the absorption coefficient for ionizing radiation k is $4.5 \times 10^3 \text{ m}^{-1}$ (in accordance with [25]). The presence of negative ions is neglected since they appear in the sheath only and their concentration is much lower than that of positive ions in the case of the positive corona.

The key feature of the model used is that it enables simulating the corona discharge without applying the Kaptsov's assumption [30], Peek's empirical formula [31] or an experimental I-V curve. Thus, the numerical modeling of the discharge can be performed for any electrode shape without carrying out preliminary experiments unlike the case of many papers including recent ones, e.g., [32–34]. It is known that both secondary emission and photoionization may be seed electrons sources in positive corona [25]. Disregarding

the secondary emission can be substantiated in the following way. In positive corona, the secondary emission is possible on a grounded (plane) electrode. However, the intensive attachment shortly turns emitted electrons to negative ions since the electric field strength near the grounded plane does not exceed 3 kV cm^{-1} . Thus, the secondary emission provides negative ions flux from the plane to the needle instead of that of electrons. It is possible to turn negative ions back to electrons ("detachment"); however, a strong electric field strength (approximately 60 kV cm^{-1} according to [25]) is necessary. To estimate whether the detachment and the secondary emission should be taken into account, one can assess whether the detachment might be sufficient beyond the ionization zone obtained in the considered model (where photoionization is the only seed electrons source). One may estimate the border of ionization zone by the ratio of the impact ionization intensity to that of photoionization. The ratio of intensity of the impact ionization to photoionization intensity reaches 10 at $140 \mu\text{m}$ from the tip (Fig. 1). Inside this zone, variations in seed electrons sources are negligibly small in comparison to the impact ionization. Meanwhile, the electric field strength sufficient for detachment (60 kV cm^{-1}) is obtained in the model at the distance of $100 \mu\text{m}$ from the needle tip—inside the ionization zone. Thus, the secondary emission (with consequent detachment) fails to compete with the photoionization as a seed electrons source and may be excluded from the consideration. The set of equations (2)–(6) is supplemented with hydrodynamics equations (7)–(8) to describe airflow:

$$\rho \partial \mathbf{V} / \partial t + \rho (\mathbf{V}, \nabla) \mathbf{V} = -\nabla P + \eta \nabla^2 \mathbf{V} + en_i \mathbf{E} \tag{7}$$

$$\text{div}(\mathbf{V}) = 0. \tag{8}$$

Here \mathbf{V} is the air velocity, P is the pressure, ρ is the mass density, and η is the dynamic viscosity.

Electrons concentration contributes to the Coulomb force as well as ions concentration. However, electrons concentration is less than 1% of ions concentration in any point of the considered air bulk. Therefore, electrons contribution to the Coulomb force would not significantly influence the Coulomb force distribution and it was not taken into account. The hydrodynamics equations (7)–(8) describe incompressible laminar flow with viscosity. The assumption of incompressibility is based on the sufficient condition $V/V_s \ll 1$ where V_s is the sonic speed: air velocity V in the solution does not exceed 10 m s^{-1} , which corresponds to $V/V_s = 1/30$. The Reynolds number can be estimated as $\text{Re} = \rho V D / \eta \approx 10^3$ where D is the needle diameter. Flows with such a low order of Re can be described as laminar. It was also checked in experiments that noticeable chaotic fluctuations of velocity are absent.

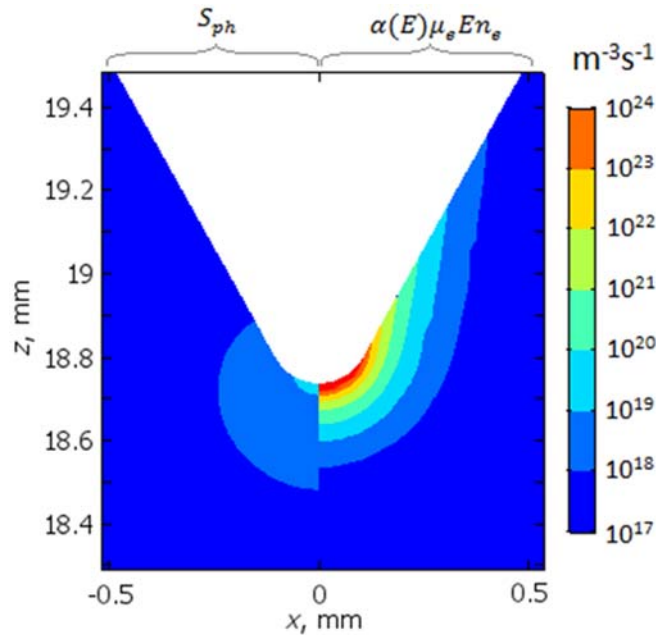


Fig.1. Photoionization and impact ionization source terms for equation (4). The vertically oriented needle (inclination angle β is 0°). Voltage 6.8 kV , electric current $1.0 \mu\text{A}$.

The geometry of the computational domain is shown in Fig. 2. A 3D model is implemented since the system has neither 2D nor 2D axial symmetry; however, there is a symmetric plane, which was used to reduce

computational costs since solving such a 3D problem is quite a resource-intensive task. The angle of inclination β is varied from 0 to 90° with the position of the needle tip being fixed. Consequently, the needle length between its tip and model boundary varies in the computational model. Nevertheless, it is an acceptable adjustment since geometric features of the needle holder has nearly no effect on the ionic wind as well as on the corona discharge per se. The shape of the needle is a cylinder with a conical end like it is shown in Fig. 2 (a). The diameter of the needle base is 0.7 mm; the conical end length is 1.3 mm; the curvature radius of the conical end is 0.12 mm.

The boundary conditions are summarized in Table 1. U is the electric potential value at the high voltage electrode, N denotes the normal to the boundary. Boundary conditions for electrons on the high-voltage electrode “A” and for ions on the grounded electrode “C” are trivial: particle fluxes formulation in these boundary conditions coincide with the formulation in the bulk equations (4) and (5). Such a boundary condition setting allows avoiding the necessity to resolve thin diffusive layers on electrodes that thickness is negligibly small. The diffusion layer thickness may be estimated as $D_{e,i}/\mu_{e,i}E$ and does not exceed 1 μm at the needle and 10 μm at the grounded plane for electrons. For ions, the diffusion layer thickness is at least one order of magnitude smaller. A convergence control ensures that the resulting numerical task is a well-posed one.

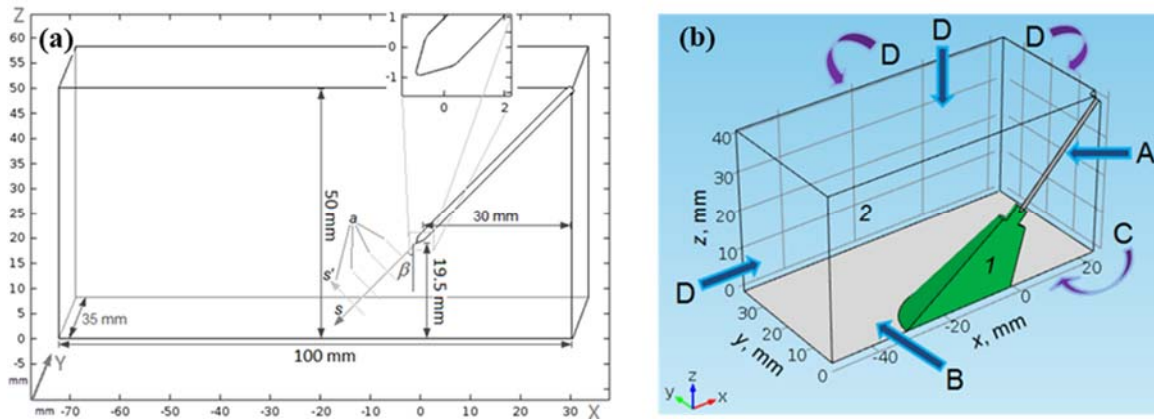


Fig.2. Model geometry with paths for linear plots (a) and boundary indexes (b) used in Table1.

Table 1. Boundary conditions. Boundary indexes "A"–"D" are introduced in Fig. 2.

Equation #	"B"–the symmetry plane	"C"–the grounded electrode	"D"–the external boundary	"A"–the high voltage electrode
(2)–(3)	$\partial\varphi/\partial y = 0$	$\varphi = 0$	$(E, N) = 0$	$\varphi = U$
(4)	$\partial n_e/\partial y = 0$	$(-D_e \nabla n_e - n_e \mu_e E) \cdot N = 0$		$j_{e,N} = -D_e \nabla n_e - n_e \mu_e E_N$
(5)	$\partial n_i/\partial y = 0$	$j_{i,N} = -D_i \nabla n_i + n_i \mu_i E_N$	$(-D_i \nabla n_i + n_i \mu_i E) \cdot N = 0$	
(6)	$\partial S_{ph}/\partial y = 0$	$\partial S_{ph}/\partial n = 0$	$\partial S_{ph}/\partial n = 0$	$\partial S_{ph}/\partial n = 0$
(7)–(8)	$V_y = 0$	$V = 0$	$-PN + \eta \nabla V = \mathbf{0}$ ("open boundary")	$V = 0$

The computation uses software package COMSOL Multiphysics® based on the finite element method. The set of equations (2)–(6) is calculated as a transient problem until the steady-state regime is obtained. The air bulk is split into the domain where high velocity is observed and the domain where air velocity is low (Fig. 2). A uniform triangular mesh is built in the high-velocity-domain. The element size is decreasing gradually towards the needle tip. A mapped mesh is built in a 0.1 mm-layer encircling the needle. Boundary layers are built on the grounded electrode surface. A boundary layer at the needle surface is used to resolve thin details of the ionization zone. The layer's thickness is 100 μm , which includes the ionization zone. The reciprocal ionization coefficient out of the layer exceeds 1 mm, which defines characteristic spatial size for concentration gradients. The element size in the layer is between 3 and 15 μm . The computation time lies within 4 hours for one voltage value at Intel i7 CPU (3.4 GHz). The total number of elements is above 500000, which corresponds to 1100000 degrees of freedom solved for. To ascertain the solution to be mesh independent, a separate investigation was

undertaken, and reducing element sizes by a factor of 1.5 (i.e., approximately twofold increase in the number of elements) was found to change the solution in the most important area (near the needle tip) by less than 1% (though some greater differences were found far away from the tip).

3. Results and discussion

3.1 Current-voltage characteristics

In the experiment, a DC voltage source was used to maintain the corona discharge. The voltage was applied to the needle electrode, while the plane one (which size was $190 \times 110 \times 6$ mm) was grounded. Experimental set-up provided an opportunity to measure current and voltage values using measuring resistance and an analog-to-digital converter. In the computer simulation, the electric current was evaluated by integrating the ion flux over the grounded electrode (plane) surface. The latter equals the integral of the electron flux over the needle electrode due to using the steady-state solution. The observed and computed current-voltage characteristics for the vertically oriented needle have a classical parabolic shape (Fig. 3). The calculation is in good agreement with the experiment except for the range from 6.5 to 7 kV where streamers were observed in the experiment. Positive corona may issue in a streamer form near (about 1 kV) the threshold voltage with short weak streamer channels which causes short current pulses [35]. Our simulation does not describe the streamer phenomena, which may be the reason for the difference in current-voltage characteristics at 6-7 kV.

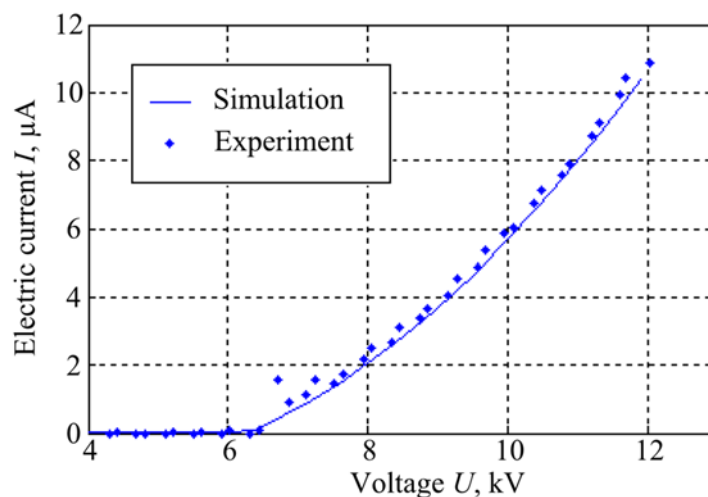


Fig. 3. Experimental and numerical current-voltage characteristics for the vertically oriented needle (inclination angle β is 0°).

In the considered system, the needle inclination affects the current-voltage characteristics (Fig. 4), though the threshold voltages for all cases coincide within the measurement error—the extrapolation of I/U vs. U dependency unto crossing with the abscissa axis shows the onset voltage U_0 to be 6.0 ± 0.1 kV. The inclination reduces the electric current value up to 30% at the constant voltage when the inclination varies from 0° to 90° . One of the possible explanations of the latter is the following. When the needle is vertically oriented, the electric field distribution along its bottom part (and the tip, in particular) is similar to that of a sphere electrode; consequently, the electric field strength is in inverse proportion to the squared tip radius. However, the strength near the electrode bottom part (except the very tip) is in inverse proportion to the first power of the needle radius when the needle is horizontally oriented since the electrode arrangement is like a wire-plane one. The above should lead to the decrease in the electric current since the ionization intensity is highly dependent on the electric field strength. The computer simulation succeeds to describe the key features of the current-voltage characteristics: the total electric current rises with increasing the inclination whereas the threshold voltage is independent of the tilt. Quantitatively computed threshold voltages (5.95 ± 0.1 kV) are in good agreement with experimental ones (6.0 ± 0.1 kV). However, the electric current values are in good agreement for $\beta = 0^\circ$ only whereas for $\beta = 90^\circ$ the difference reaches 15%, which may be considered as a satisfactory agreement, especially, regarding the absence of any empirical suggestions introduced to the model.

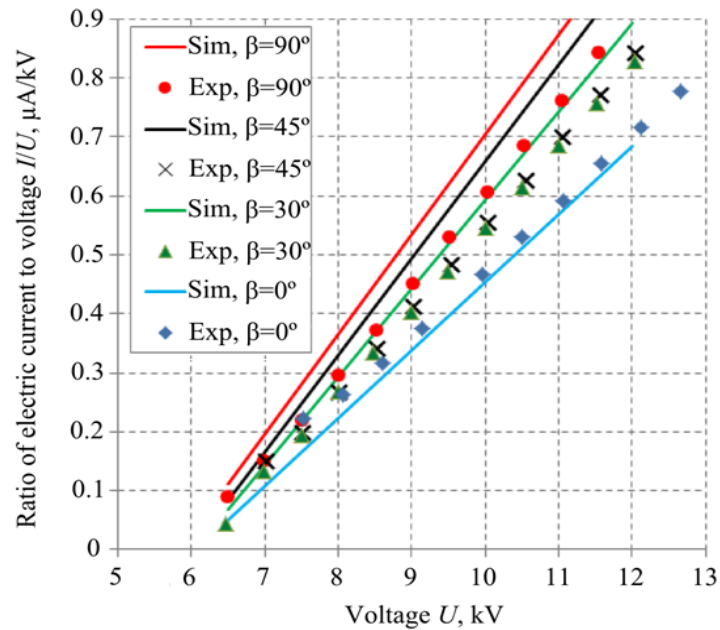


Fig. 4. I/U vs. U dependencies: comparison of the experiment (“Exp”) and simulation (“Sim”). Needle inclination β is varied.

3.2 Influence of the inclination on flow velocity field

Velocity field distributions were observed using LaVision FlowMaster equipment based on the particle image velocimetry (PIV-method) [36]. The investigated area was filled with seeding particles— aerosol of $C_{26}H_{50}O_4$ —that has a small droplet size and do not change studied parameters significantly. Laser beam plate was configured to light the needle tip and flow jet area. According to the PIV technique, two consecutive frames were recorded with a tiny delay. Then, images were processed using a two-dimensional cross-correlation algorithm to restore the velocity distribution in the plane of a laser beam. Since the flow structure is the steady-state, statistical evaluation was performed using several data sets. Original experimental results are presented and discussed in [19]. The calculated and experimental flow patterns are presented in Fig. 5 for inclinations: $\beta = 0^\circ$, $\beta = 45^\circ$ and $\beta = 90^\circ$. The flow form is a thin jet. The jet is directed from the needle and approximately coincides with the needle axis. It is obtained on closer inspection that air jet wraps down to the grounded plane at $\beta = 90^\circ$.

The velocity profiles (Fig. 6) show that the thickness of the jet (at a level of 50% of the maximum speed) is about 2 mm. The maximum gradually decreases when moving away from the needle. Experimental and computational results are in a good agreement. However, some overestimation of the velocity peak near the needle is observed. Also, the side stream which flows along the ground electrode surface to the right is weaker in the simulation than in the experiment (Fig. 5). These discrepancies may indicate that simulation underestimates moving force of peripheral ions in relation to moving force of ions near the needle tip. It may indicate the variation of ion mobility (that is considered to be constant in the numerical model) in the interelectrode gap, which is discussed, in particular, in [37]. The airflow is not ideally straight, so the formal definition of jet direction θ is presented in Fig. 5b: the point of maximum air velocity on the distance of 18 mm from the needle edge is considered and the jet direction θ is the angle between the vertical direction and the segment connecting this point and the needle tip.

According to Fig. 7 (a), the jet direction is nearly independent of the voltage for $\beta = 90^\circ$; the conclusion is also valid for other values of β . The direction of the jet is an intermediate one between the vertical line and the direction of the needle axis. Larger needle inclination β leads to the larger difference between the needle axis and airflow direction (Fig. 7 (b)).

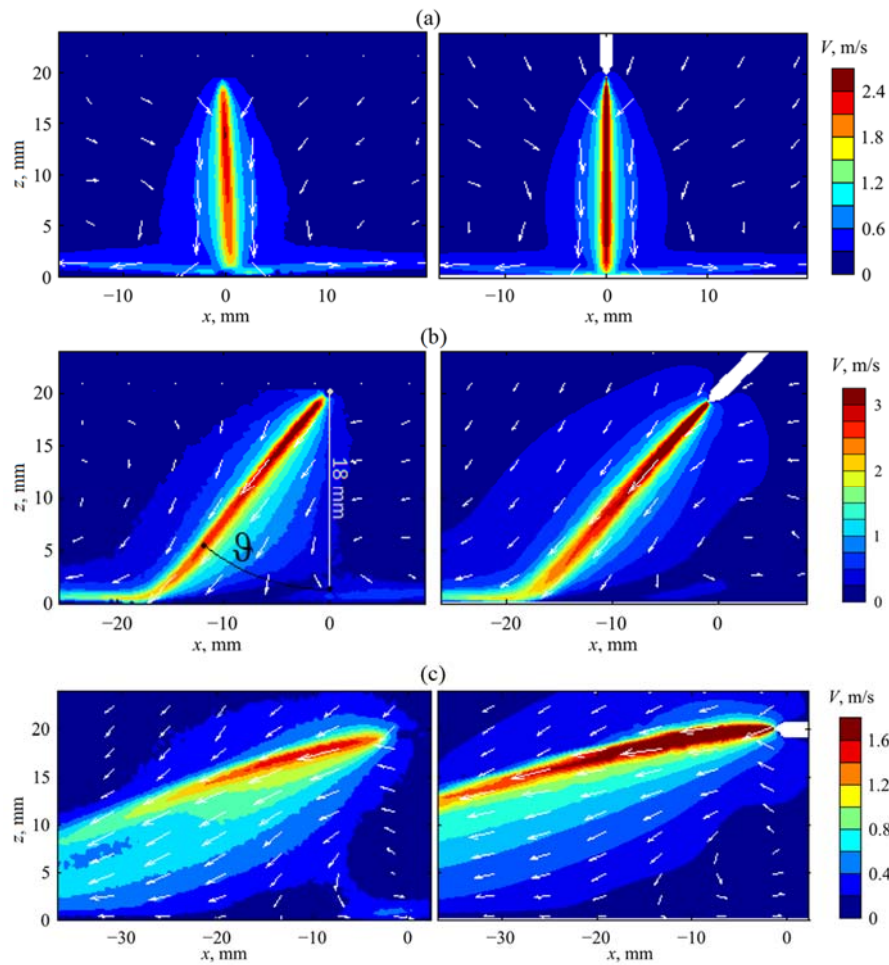


Fig. 5. Airflow velocity distributions in XZ-plane (the symmetry plane): the comparison of the experiment (on the left) and the simulation (on the right). (a) needle inclination $\beta = 0^\circ$, corona discharge current $I = 1.1 \mu\text{A}$, voltage $U = 6.8 \text{ kV}$; (b) $\beta = 45^\circ$, $I = 1.3 \mu\text{A}$, $U = 7.2 \text{ kV}$; (c) $\beta = 90^\circ$, $I = 1.1 \mu\text{A}$, $U = 7.3 \text{ kV}$.

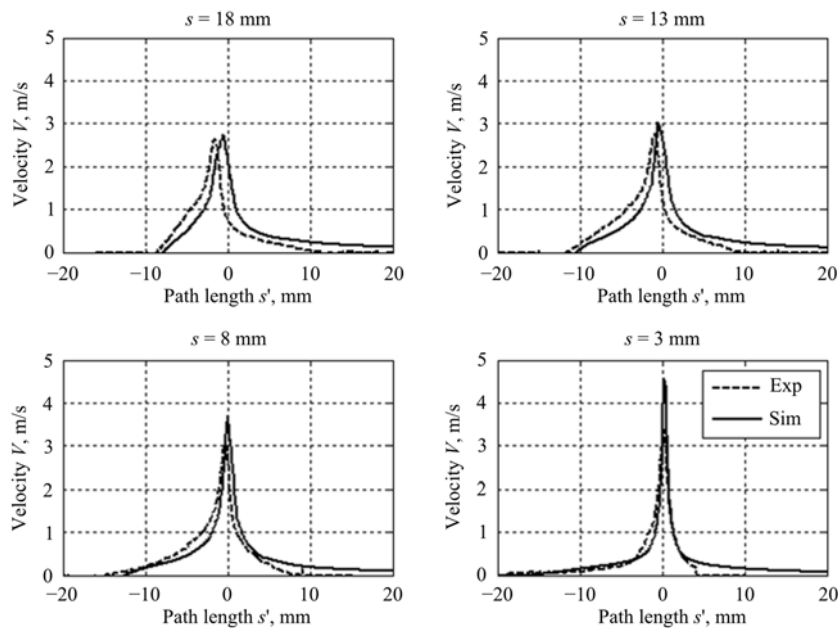


Fig. 6. Velocity profiles for various distances s from the needle tip along paths shown in Fig. 2 (a): the experimental (“Exp”) and simulation (“Sim”) data. Inclination angle $\beta = 45^\circ$; current $I = 1.3 \mu\text{A}$, voltage $U = 7.2 \text{ kV}$.

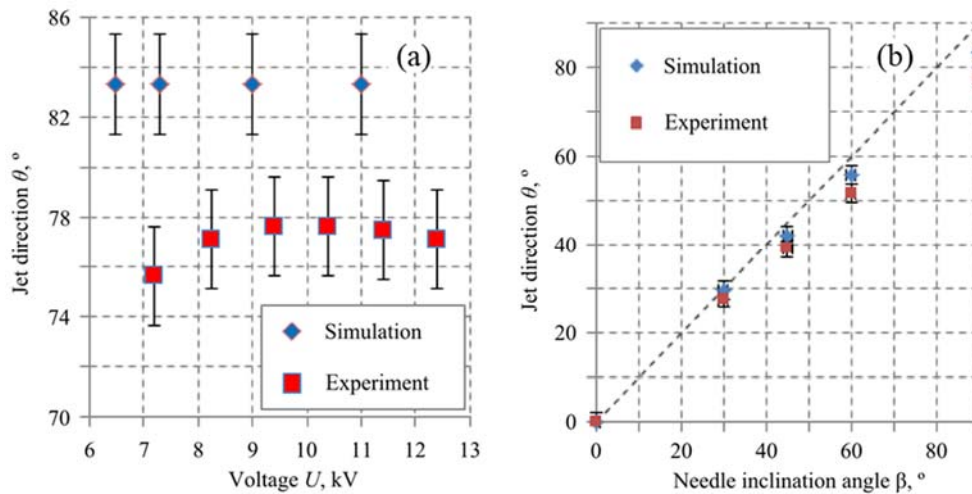


Fig. 7. (a) jet direction angle θ vs. voltage U for needle inclination $\beta = 90^\circ$; (b) jet direction angle θ vs. needle inclination angle β for voltage $U = 7.3$ kV.

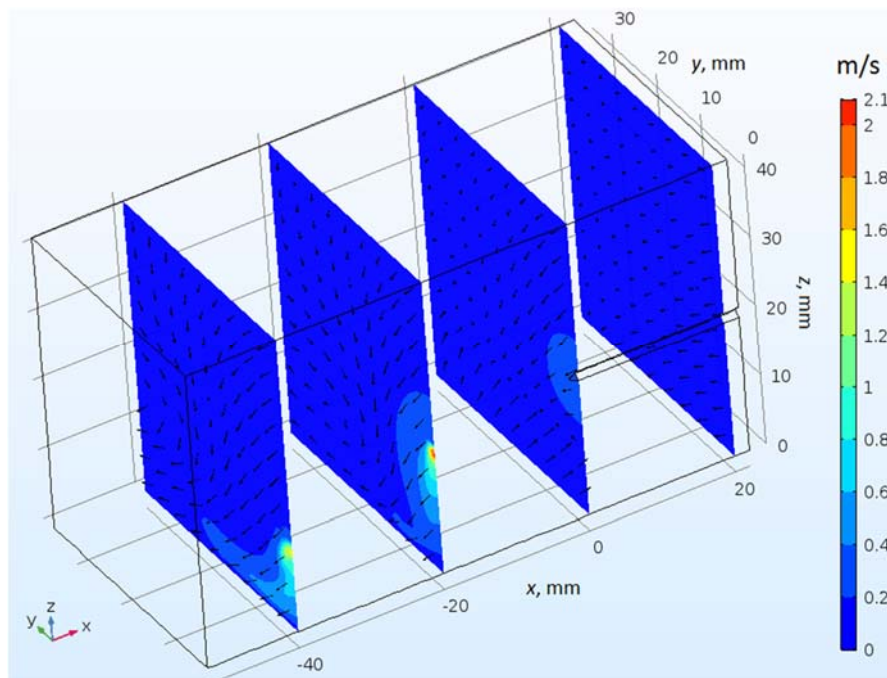


Fig. 8. The arrow and contour plot of velocity for inclination angle $\beta = 90^\circ$, electric current $I = 1.1 \mu\text{A}$, and voltage $U = 7.3$ kV.

The maximum difference between the needle axis and electrohydrodynamic jet direction is observed for inclination $\beta = 90^\circ$. As mentioned above, the discrepancy may be related to the lower mobility of ions that are far from the corona sheath. Such inequality of mobilities far and near to corona sheath would increase the Coulomb force near the grounded electrode (in accordance to (1)), which turns the jet to the grounded plane. There is no axial symmetry in airflow for $\beta > 0^\circ$. The general structure of the flow remains the following: a narrow jet with vortexes sideways. If the inclination is strong ($\beta = 90^\circ$), vortexes in YZ-plane are more expressed than in YZ-plane (Fig. 8).

3.3 The Coulomb Force Analysis

Since the effect of inclining needle to the jet tilt is reproduced in the computer model, an analysis of the effect can be made by the simulation results. Electric field lines are perpendicular to the surface of the electrode, so the needle direction determines the direction of electric field vectors near the tip (Fig. 9 (a) and (c)). It is here

where the electric field intensity is the largest, and therefore it is here where the Coulomb force is the largest. Fig. 9 (b) and d shows that the Coulomb force is concentrated in a narrow region near the tip of the needle. Coulomb force of a sphere built around the center at the needle tip may be calculated as:

$$F_C(R) = \iiint_{x^2+y^2+(z-H)^2 < R^2} e(n_+(x, y, z) - n_-(x, y, z))\mathbf{E}(x, y, z)dx dy dz \quad (9)$$

Here R is the sphere radius, H is the interelectrode distance. The following results are obtained for the model with inclination $\beta = 90^\circ$, $I = 1.1 \mu\text{A}$, $U = 7.3 \text{ kV}$. For the whole bulk ($R = \infty$) integration (9) gives a force which z -component is 1.4 times as much as its x -component: it means that the total force is turned at an angle of 55° relative to the needle. However, for the sphere with $R = 3 \text{ mm}$, the integration (9) gives the force that z -component is six times smaller than its x -component; thus, the force is almost co-directional with the needle axis. The force concentrated within the small volume is more than 10% of the total force. Such a high force density provides the generation of a thin ionic wind jet that may be hardly turned by a dispersed force in the peripheral zone. In the vicinity of the needle tip, electric field lines are diverging from the tip and do not wrap up to the ground electrode (Fig. 9 (b) and d). So, it is the electric field at the needle point, which defines the air jet direction (Fig. 9 (a) and (c)).

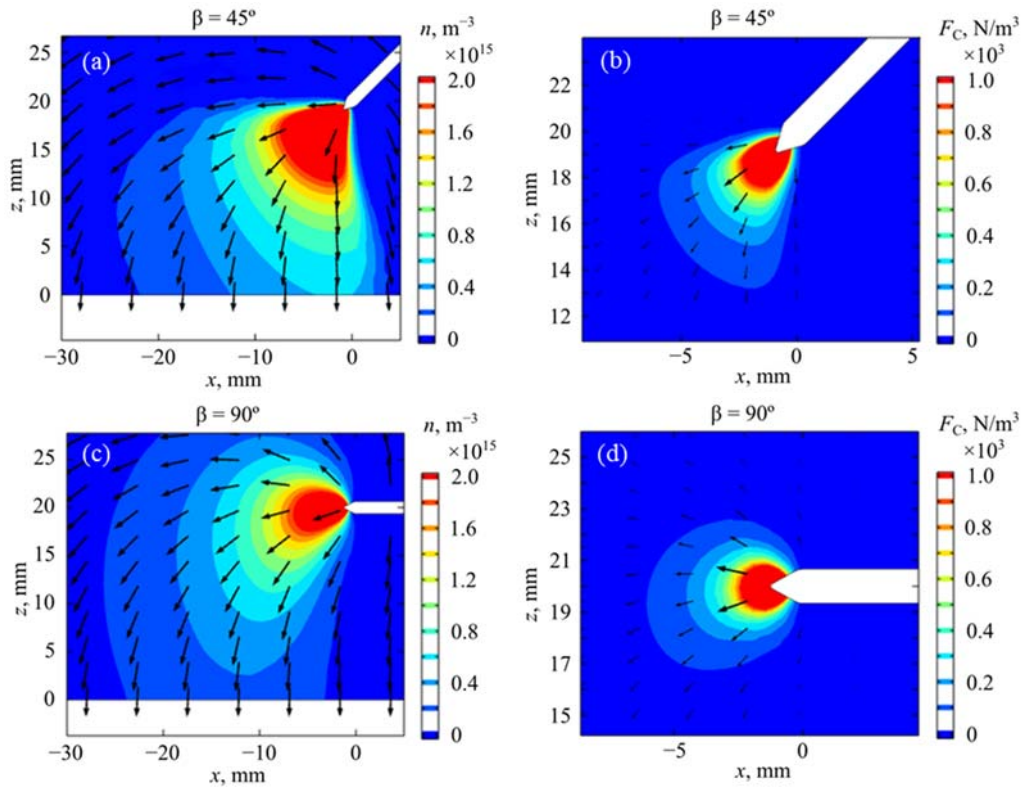


Fig. 9. The ion concentration and the Coulomb force distributions in XZ-plane (the symmetry plane) for different needle inclinations β and for voltage $U = 7.3 \text{ kV}$: (a), (c) the ion concentration (m^{-3}) (contours) and the electric field direction (arrows); (b), (d) the Coulomb force (N m^{-3}) (contours and arrows).

4. Conclusion

The ionic wind jet direction is not determined by that of the shortest path from the high-voltage electrode to the grounded one, which is because the main pulse of the jet is gained in a zone near the point of the high-voltage electrode. The Coulomb force direction coincides with that of the electric field, yielding that the electrode tip orientation strongly affects the ionic wind direction. As a result, the airflow line in the needle-plane system is close to the needle inclination (the jet direction deviates from the needle axis when the inclination is close to 90° only). Thus, one can change the ionic wind direction, varying the high-voltage electrode inclination.

Acknowledgment

Research was carried out using resources provided by the Computer Center of SPbU and Center "Geomodel" of Research park of St. Petersburg State University. This research received no specific grants from funding agencies in the public, commercial, or not-for-profit sectors.

References

- [1] Robinson M., Movement of air in the electric wind of the corona discharge, *Trans. Am. Inst. Electr. Eng. Part Commun. Electron*, Vol. 80 (2), pp. 143–150, 1961.
- [2] Yabe A., Mori Y., and Hijikata K., EHD study of the corona wind between wire and plate electrodes, *AIAA Journal*, Vol. 16 (4), pp. 340–345, 1978.
- [3] Takeuchi N., and Takubo K., Enhancement of mass transfer of reactive species by gas- and liquid- phase flow induced by corona discharge generated above water, *Int. J. Plasma Environ Sci. Technol.*, Vol. 9 (1), pp. 2–6, 2014.
- [4] Laroussi M., Nonthermal decontamination of biological media by atmospheric-pressure plasmas: Review, analysis, and prospects, *IEEE Trans. Plasma Sci.* Vol. 30 (4), pp. 1409–1415, 2002.
- [5] Chen I.Y., Chen C.-J., and Wang C.-C., Influence of electrode configuration on the heat transfer performance of a LED heat source, *Int. J. Heat Mass Transfer*. Vol. 77, pp. 795–801, 2014.
- [6] Lee S.J., Li L., Kwon K., Kim W., and Kim D., Parallel integration of ionic wind generators on PCBs for enhancing flow rate, *Microsystem Technologies*. Vol. 21 (7), pp. 1465–1471, 2015.
- [7] Wang J., Cai Y.-X., Li X.-H., Shi Y.-F., and Bao Y.-C., Electrically-induced ionic wind flow distribution and its application for LED cooling, *Appl. Therm. Eng.* Vol. 138, pp. 346–353, 2018.
- [8] Qu J., Kong L., and Zhang J., Experimental investigation on flow and heat transfer characteristics of a needle-cylinder type ionic wind generator for LED cooling, *Energies*. Vol. 11 (5), pp. 1149, 2018.
- [9] Benard N., and Moreau E., Electrical and mechanical characteristics of surface AC dielectric barrier discharge plasma actuators applied to airflow control, *Exp. Fluids*, Vol. 55, pp. 1846, 2014.
- [10] Borghi C.A., Carraro M.R., Cristofolini A., and Neretti G., Electrohydrodynamic interaction induced by a dielectric barrier discharge, *J. Appl. Phys.*, Vol. 103 (6), pp. 063304, 2008.
- [11] Moreau E., Airflow control by non-thermal plasma actuators, *J. Phys. D: Appl. Phys.*, Vol. 40 (3), pp. 605–636, 2007.
- [12] Rickard M., Dunn-Rankin D., Weinberg F., and Carleton F., Maximizing ion-driven gas flows, *J. Electrostat.*, Vol. 64. pp. 368–376, 2006.
- [13] Khomich V.Y., and Rebrov I.E., In-atmosphere electrohydrodynamic propulsion aircraft with wireless supply onboard, *J. Electrostat.*, Vol. 95, pp. 1–12, 2018.
- [14] Ianconescu R., Sohar D., and Mudrik M., An analysis of the Brown-Biefeld effect, *J. Electrostat.*, Vol. 69. pp. 512–521, 2011.
- [15] Moreau E., Benard N., Lan-Sun-Luk J.-D., and Chabriat J.-P., Electrohydrodynamic force produced by a wire-to-cylinder dc corona discharge in air at atmospheric pressure, *J. Phys. D: Appl. Phys.*, Vol. 46 (47), pp. 475204, 2013.
- [16] Moreau E., Benard N., Alicalapa F., and Douyère A., Electrohydrodynamic force produced by a corona discharge between a wire active electrode and several cylinder electrodes - Application to electric propulsion, *J. Electrostat.*, Vol. 76, pp. 194–200, 2015.
- [17] Elagin I.A., Yakovlev V.V., Ashikhmin I.A., and Stishkov Yu. K., Experimental investigation of cooling of a plate by Ionic Wind from a Corona-Forming Wire Electrode, *Technical Phys.*, Vol. 61 (8), pp. 1214–1219, 2016.
- [18] Moreau E., Audier P., and Benard N., Ionic wind produced by positive and negative corona discharges in air, *J. Electrostat.*, Vol. 93, pp. 85–96, 2018.
- [19] Elagin I.A., Begal' D.I., Ashikhmin I.A., and Stishkov Yu.K., Change in the direction of electric wind from a wire electrode tilted relative to a grounded plane, *Technical Phys. Lett.*, Vol. 43 (1), pp. 98–100, 2017.
- [20] Zhao L., and Adamiak K., Numerical analysis of forces in an electrostatic levitation unit, *J. Electrostat.*, Vol. 63, pp. 729–734, 2005.
- [21] Martins A.A., and Pinheiro M.J., Modeling of an EHD corona flow in nitrogen gas using an asymmetric capacitor for propulsion, *J. Electrostat.*, Vol. 69, pp. 133–138, 2011.
- [22] Samusenko A., Stishkov Yu., and Zhidkova P., Computer simulation of ionic wind in the point-torus electrodes system, *Int. J. Plasma Environ Sci. Technol*, Vol. 9 (1), pp. 24–28, 2015
- [23] Zhidkova P.S., and Samusenko A.V., A computer model of the ionic wind in the unipolar approximation with the boundary condition on the ion flow variation rate, *Surface Eng. Appl. Electrochem.*, Vol. 52 (4), pp. 370–379, 2016.
- [24] Savel'eva L.A., Samusenko A.V., and Stishkov Yu.K., Reasons for branching of a positive streamer in a non-uniform electric field, *Surface Eng. Appl. Electrochem*, Vol. 49 (2), pp. 125–135, 2013.
- [25] Raizer Y.P., Kisin V.I., and Allen J.E., *Gas Discharge Physics*. Berlin: Springer, 2011.

- [26] Luque A., Ebert U., Montijn C., and Hundsdorfer W., Photoionization in negative streamers: Fast computations and two propagation modes, *Appl. Phys. Lett.*, Vol. 90 (8), pp. 081501, 2007.
- [27] Dutton J., A survey of electron swarm data, *J. Phys. Chem. Ref. Data*, Vol. 4 (3), pp. 577–856, 1975.
- [28] Gallagher J.W., Beaty E.C., Dutton J., and Pitchford L.C., An annotated compilation and appraisal of electron swarm data in electronegative gases, *J. Phys. Chem. Ref. Data*, Vol. 12 (1), pp. 109–152, 1983.
- [29] Kioussis K. N., Moronis A. X., and Fruh W. G., Electro-hydrodynamic (EHD) thrust analysis in wire-cylinder electrode arrangement, *Plasma Science and Technology*, Vol. 16 (4), pp. 363–369, 2014.
- [30] Kaptsov N., *Elektricheskiye yavleniya v gazakh i vacuume*. Moscow: OGIZ, 1947.
- [31] Peek F.W., *Dielectric Phenomena in High Voltage Engineering*. New York: McGraw-Hill, 1929.
- [32] Bedolla P.O., Vorlaufer G., Sequard-Base P., Vernes A., Franek F., Altitude dependence of electrohydrodynamic flow in an electrostatic lifter, *J. Electrostat.*, Vol. 87, pp. 32–44, 2017.
- [33] Ramadhan A.A., Kapur N., Summers J.L., and Thompson H.M., Performance and flow characteristics of miniature EHD air blowers for thermal management applications, *J. Electrostat.*, Vol. 93, pp. 31–42, 2018.
- [34] Tsui Y.-Y., Huang Y.-X., Lan C.-C., Wang C.-C., A study of heat transfer enhancement via corona discharge by using a plate corona electrode, *J. Electrostat.*, Vol. 87, pp. 1–10, 2017.
- [35] Stishkov Yu. K., Samusenko A. V., and Ashikhmin I. A., Corona discharge and electrogasdynamic flows in the air, *Physics-Uspokhi*. Vol. 61 (12), pp. 1213, 2018.
- [36] Raffel M., Willert C.E., Wereley S.T., and Kompenhans J., *Particle image velocimetry: A practical guide*, second edition. Berlin: Springer, 2007.
- [37] Melnikova N., Samusenko A., and Safronova Iu., Computer simulation of corona discharge: charge carries in external zone, in *IEEE 2nd Int. Conf. Dielectr.*, Budapest, Hungary, pp. 1–4, 2018.